Clays and Clay Minerals, Vol. 58, No. 4, 532–541, 2010.

COLLOID DIFFUSION IN COMPACTED BENTONITE: MICROSTRUCTURAL CONSTRAINTS

MICHAEL HOLMBOE*, SUSANNA WOLD, AND MATS JONSSON

KTH School of Chemical Science and Engineering, Nuclear Chemistry, Royal Institute of Technology, SE-100 44 Stockholm, Sweden

Abstract—In Sweden and in many other countries, a bentonite barrier will be used in the repository for spent nuclear fuel. In the event of canister failure, colloidal diffusion is a potential, but scarcely studied mechanism of radionuclide migration through the bentonite barrier. Column and *in situ* experiments are vital in understanding colloid diffusion and in providing information about the microstructure of compacted bentonite and identifying cut-off limits for colloid filtration. This study examined diffusion of negatively charged 2-, 5-, and 15-nm gold colloids in 4-month diffusion experiments using MX-80 Wyoming bentonite compacted to dry densities of 0.6–2.0 g/cm^3. Breakthrough of gold colloids was not observed in any of the three diffusion experiments. In a gold-concentration profile analysis, colloid diffusion was only observed for the smallest gold colloids at the lowest dry density used (estimated apparent diffusivity $D_a \approx 5 \times 10^{-13}$ m^2/s). The results from a microstructure investigation using low-angle X-ray diffraction suggest that at the lowest dry density used, interlayer transport of the smallest colloids cannot be ruled out as a potential diffusion pathway, in addition to the expected interparticle transport. In all other cases, with either greater dry densities or larger gold colloids, compacted bentonite will effectively prevent diffusion of negatively charged colloids due to filtration.

Key Words—Colloid Filtration, Compacted Bentonite, Gold Colloids, Diffusion, Microstructure, Nuclear Waste Disposal.

INTRODUCTION

Compacted bentonite is to be used as a barrier in repositories for spent nuclear fuel in several countries. The low hydraulic permeability and the great cation affinity of compacted bentonite will prevent or slow possible transport of radionuclides, in particular multivalent cationic actinides. Whereas the diffusion of radionuclides in water-saturated compacted bentonite is well documented, studies on colloid-facilitated transport of radionuclides are scarce due to the assumption that the compacted bentonite poses a sufficient barrier to colloid diffusion. However, this remains to be proven. In the event of canister failure, radiocolloids can be formed in close proximity to the fuel. Furthermore, the bentonite contains a small amount of organic material which can be leached out in colloidal form and bind cationic radionuclides (Vilks *et al.*, 1998).

In order to assess the possibility of colloid breakthrough, experimental studies are needed on the diffusion of colloids in compacted, water-saturated bentonite. Whether the microstructure of bentonite provides an efficient cut-off limit regarding colloid size is an important piece of information to establish.

Diffusion studies using small monodisperse colloid tracers of different sizes can thus contribute to understanding the microstructure of water-saturated compacted bentonite, in combination with other techniques such as neutron and X-ray small-angle scattering and diffraction (Kozaki *et al.*, 1998; Devineau *et al.*, 2006). Wold and Eriksen (2007) studied the diffusion of organic humic and lignosulphonate colloids and found unexpectedly that both colloids diffused through bentonite with an apparent diffusivity of ~10^{-12} m^2/s, irrespective of the dry density of the bentonite. The same study examined the diffusion of Eu(III) and Co(II) in the presence of humics and found drastically increased diffusivities of both ions. The apparent sorption coefficient, K_d, decreased accordingly, indicating that the humic colloids not only diffused through the compacted bentonite but also enhanced radionuclide transport.

Iijima *et al.* (2009) studied diffusion of humic acid through compacted bentonite (1.2–1.6 g/cm^3) as a function of ionic strength (0.001–1 M NaCl). Diffusion of humic acid was only found for dry densities 1.2–1.6 and 1.2–1.5 g/cm^3 at high ionic strengths corresponding to 1 and 0.1 M NaCl, respectively. Using size exclusion chromatography (SEC), Iijima *et al.* (2009) concluded that the humic acid belonged to smaller size fractions, with corresponding sizes of <5 and <3 kDa, respectively. Similarly to the study by Wold and Eriksen (2007), Nd(III) transport was found to be facilitated by the presence of humic acid.

Nowak (1984) investigated diffusion of citrate-reduced 16-nm gold colloids in low-density bentonite (0.9 g/cm^3) water-saturated with a high-ionic-strength brine solution in a column experiment. The experiment

* E-mail address of corresponding author:
holmboe@kth.se
DOI: 10.1346/CCMN.2010.0580408

https://doi.org/10.1346/CCMN.2010.0580408 Published online by Cambridge University Press

only lasted 17 days and the results indicated very slow transport of gold colloids. Due to the inconclusive results, the author recommended further experimental studies on filtration effects in compacted water-saturated bentonite. The gold colloids used are not expected, however, to be stable at the high ionic strength used in that experiment (Enüstün and Turkevich, 1963).

Kurosawa and Ueta (2001) studied gold colloid diffusion in bentonite/sand mixtures of different densities and sand content in a column experiment using partially aggregated gold colloids of 15–50 nm in size. The gold colloids were stabilized with 0.5 wt.% polyoxyethylene hydrogenated castor oil in 10% ethanol, leading to 'water-like' surface properties and sterical stabilization. No concentration profile analysis was presented but scanning electron microscopy and electron probe micro-analysis images showed that the gold colloids were deposited readily in the water-bentonite interface and thus effectively filtered by the bentonite/sand microstructure. The pressure gradient of 9×10^5 Pa used in the experiment might have affected the bentonite microstructure by facilitating pore constrictions, thereby enhancing colloid precipitation. Furthermore, non-ionic polymers can adsorb to and change the surface properties of the bentonite (Luckham and Rossi, 1999, and references therein). These results must be confirmed by further studies.

From the aspect of colloid filtration, a cut-off limit in colloid size is expected. This cut-off limit would reflect the bentonite microstructure and should depend on the compaction and the resulting size of the interlayer distances, as well as possible interparticle voids. For colloid sizes above this cut-off limit, which intuitively should decrease with increasing compaction, diffusive transport would not be possible.

The interlayer spacings of montmorillonite in a Na-dominated, water-saturated bentonite at low ionic strength depends primarily on water content. Swelling in water generally first proceeds by uptake of 1–3 (or 4) discrete water layers, known as crystalline or discrete swelling. Interestingly, the crystalline swelling of homoionic Na- or Ca-montmorillonites never seems to exceed three water layers (Norrish, 1954; Kozaki *et al.*, 1998), whereas MX-80 bentonite can undergo uptake of 4 water layers during crystalline swelling (Saiyori *et al.*, 2004). Regarding colloid diffusion, interlayer transport would not be possible when crystalline swelling dominates the microstructure as the average interlayer distance would be ~1 nm or smaller (Norrish, 1954; Kozaki *et al.*, 1998; Saiyouri *et al.*, 2004). At very high dry densities, colloid diffusion would thus only be possible in connected interparticle voids, if such exist.

Increasing the water content further in bentonite results in the formation of diffuse double layers between the montmorillonite layers and a consequent jump in the interlayer thickness from 3 or 4 water layers (interlayer distances of 0.9 to ~1.2 nm, respectively) to >10 water layers (>3 nm). The second type of swelling (Norrish, 1954) is referred to hereafter as osmotic swelling. The interlayer distances in water-saturated bentonite can be obtained from the basal spacing, d_{001}, using low-angle X-ray diffraction (XRD) for example, where the interlayer distance is the basal spacing minus the thickness of one montmorillonite layer, ~0.95 nm. Due to certain diffraction effects occurring for small interstratified particles at low angles (<5º2θ), the true interlayer spacing might be slightly different than the interlayer distances obtained directly from Bragg's law (Moore and Reynolds, 1997; Janeba *et al.*, 1988; Vaia and Liu, 2002). Note also that a certain distribution of basal spacings will always exist, even at small water contents (Ferrage *et al.*, 2005).

Regarding the terminology, differentiation between interlayer and interparticle voids is important, as the interlayer voids may have different size, geometry and surface properties compared with interparticle voids. Even for two montmorillonite layers subjected to osmotic swelling and separated by >~3 nm, the corresponding void should be termed an interlayer void in order to avoid confusion with the interparticle voids.

In the context of diffusion of colloids in bentonite, positively charged colloids are expected to undergo deposition and strong sorption onto the negatively charged clay surfaces, and hence have very little mobility. Stable neutral colloids with 'water-like' surface properties, as in the Kurosawa and Ueta (2001) study, are uncommon among inorganic colloids. In the present study, negatively charged colloids were, therefore, chosen to investigate possible diffusion of inorganic colloids in compacted bentonite.

Diffusion of negatively charged colloids in interparticle voids and possible connected networks of these voids could also be affected by electrostatic repulsion by the negatively charged surfaces and edges of the clay particles (Secor and Radke, 1985; Tombácz and Szekeres, 2004), which would further reduce the active volume available for diffusion. In order to decrease the impact of this effect, the ionic strength should be as great as possible, without severely reducing colloid stability.

The objective of the present experimental study was to investigate colloid diffusion in compacted bentonite, using an identical experimental diffusion setup as used by Wold and Eriksen (2007) (Figure 1) and smaller colloids than in the study by Kurosawa and Ueta (2001). Gold colloids of sizes 2, 5, and 15 nm were chosen because they have well defined geometry and size and a narrow size distribution, and are chemically inert.

Gold colloid concentrations in the diffusion and concentration profile experiments were analyzed using inductively coupled plasma optical emission spectrometry (ICP-OES) at 267.594 nm. For the 5-nm and 15-nm gold colloid solutions, the colloid stability was monitored using ultraviolet-visible (UV-Vis) spectroscopy.

https://doi.org/10.1346/CCMN.2010.0580408 Published online by Cambridge University Press

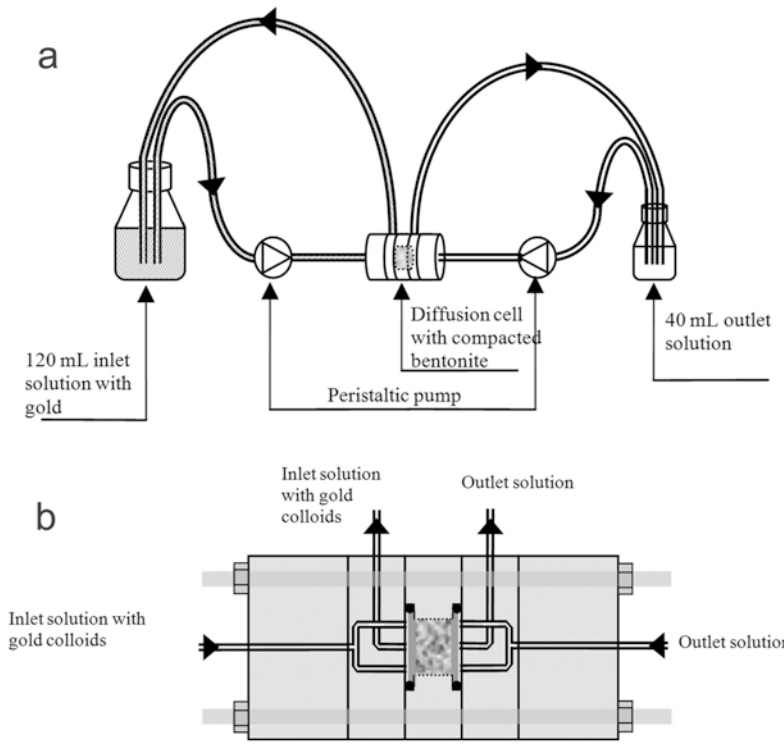


Figure 1. (a) Schematic illustration of the diffusion experiment setup. (b) Schematic illustration of the diffusion cell.

Furthermore, the microstructure and the interlayer distances of the water-saturated bentonite at dry densities of 0.5−1.0 g/cm^3 were investigated by low-angle XRD.

MATERIALS AND METHODS

Gold colloids

Gold colloid solutions were obtained from BB International (Madison, Wisconsin, USA). The manufacturer's quality control revealed average sizes of 5.5 and 14.3 nm for the 5- and 15-nm gold colloids, with coefficients of variance of <15% and <10%, respectively. The quality of the 2-nm gold colloids was verified by measuring the absorbance at 400 nm, because 2-nm gold colloids are too small to give rise to the surface plasmon effect and are, therefore, colorless. According to the manufacturer, the gold colloid stock solutions contain little or no residual $AuCl_4^-$.

Bentonite clay

MX-80 Wyoming bentonite with a montmorillonite content of ~82% was used without further treatment. The exchangeable cations for this bentonite are approximately: 74.8% Na^+, 16.7% Ca^{2+}, 6.7% Mg^{2+}, and 2% K^+. The CEC measured by the trien-Cu(II) method is 0.75 meq/g (Karnland *et al.*, 2006).

Gold colloid stability

To improve gold colloid stability, 3-mercaptosuccinic acid was chosen as a suitable stabilizing agent above pH 8, on the basis of a colloid stability screening test on the 5- and 15-nm gold colloids prior to the diffusion experiments. Adsorption to the gold colloid surface is anticipated through the thiol group *via* chemical adsorption (Zhu *et al.*, 2003). 3-mercaptosuccinic acid is a small, water-soluble thiol with dissociated carboxylate groups which provide the negative surface charge required to maintain colloid stability.

Because either sorption to or aggregation with bentonite would reduce the gold colloid stability, the sorption of both thiol-treated and untreated (as received) 5-nm gold colloids to bentonite was investigated. The sorption coefficient, K_d, was obtained from standard sorption batch measurements with a volume to mass ratio of 200 cm^3/g and a gold colloid concentration of 1.2 ppm as measured by ICP-OES.

During the diffusion experiments, the colloid stability in the inlet solutions was monitored using UV-Vis spectroscopy for the 5- and 15-nm gold colloids at 510 nm and 518 nm, respectively. Because 2-nm gold colloids are too small to give rise to the surface plasmon effect (>~3−4 nm), colloid stability in the 2-nm gold colloid experiment was monitored by ICP-OES. Halfway through the 15-nm gold colloid experiment, TEM images

https://doi.org/10.1346/CCMN.2010.0580408 Published online by Cambridge University Press

Table 1. Dry densities of the bentonite used in each diffusion experiment.

Gold colloids (nm)	Dry densities of bentonite in PEEK cells (g/cm^3)								
2		0.6		1.0		1.4		1.8	
5	0.5	0.6	0.8	1.0	1.2	1.4	1.6	1.8	
15		0.6	0.8	1.0	1.2	1.4	1.6	1.8	2.0

of both the inlet and outlet solutions, dried on carbon-coated copper grids, were taken using a Philips 100 kV Technai transmission electron microscope operating at 70 kV.

DIFFUSION EXPERIMENTS

All glassware and diffusion cell parts were acid washed and rinsed with Milli-Q water before the experiment. In general, bentonite was compacted uniaxially in the direction of transport to dry densities of 0.5–2.0 g/cm^3 into PEEK (Polyetheretherketone) cells with 10 mm inner diameter and 5 mm column length, confined by two metal frits with pore size 0.5 μm, held in place by O-rings (Figure 1b). The diffusion cells were equilibrated with 1 mM $NaClO_4$ solution for 2–4 months prior to the diffusion experiments. The bentonite dry density in each diffusion experiment were also measured (Table 1).

$NaClO_4$ was added to the colloid solutions to compensate for the dilution by the thiol treatment in order to maintain an ionic strength corresponding to 1 mM $NaClO_4$ solution. The final gold colloid concentrations, C_0, in the inlet solutions, the 3-mercaptosuccinic acid concentrations, the pH, and the conductivities were also measured (Table 2).

The concentrations of gold were analyzed using a Varian Vista AX ICP-OES instrument at 267.594 nm, with a gold detection limit at low ppb concentrations. All samples were handled gravimetrically. To ensure that the gold colloid concentration in the outlet solutions was correct, duplicate samples were taken to account for possible residual $AuCl_4^-$ from the gold colloid stock solutions (Kurosawa and Ueta, 2001). One sample was filtered with a 10 kDa MWCO Vivaspin ultrafilter (Vivaproducts, Littleton, Massachusetts, USA) with approximate pore size of 1.33 nm according to the supplier. The measured concentration of the filtered sample, $C_{t,\ filtered}$, was subtracted from the unfiltered sample concentration, C_t, and the remaining concentration was taken as the real gold colloid concentration, i.e. $C_t - C_{t,\ filtered} = \Delta C_{Au}$. Filtration of the 2 nm, 5 nm, and 15 nm stock solutions with 10kDa MWCO Vivaspin ultrafilters revealed that $AuCl_4^-$ could not be detected using the ICP-OES instrument, however. The residual $AuCl_4^-$ concentration, if present at all, was therefore $\leqslant 1$ ppb in the stock solutions.

To minimize the sampling volume, 1.0–2.5 mL samples from the outlet solutions were diluted to the required sample volume of 3.5–4.0 mL for the ICP-OES instrument. The sampling volume was increased during the course of the experiments. The initial dilution was made with 0.35 mL of prepared-daily *aqua regia* to acidify and dissolve possible gold colloids. The remaining dilution was achieved using Milli-Q water.

Each diffusion experiment was conducted for 4 months and samples were drawn on a weekly or biweekly basis. The inlet solution volume was 120 mL and the outlet solution volume 40 mL.

Concentration profile analysis

After completion of the diffusion experiments, the diffusion cells were dismantled and the bentonite pellets were sliced into thin slices with thicknesses increasing with increasing distance from the inlet filter. By weighing each slice, the thickness was calculated from the total weight and total length of the bentonite pellets. After the first diffusion experiment using the 15-nm gold colloids, the diffusion cells were dismantled, sliced, left to stand overnight in 2 mL of fresh *aqua regia* to dissolve any gold colloids present and then diluted to 6 mL with Milli-Q water. When the filters are removed, immediate swelling may occur if excess water is present. A suction effect might, therefore, have caused diffusion

Table 2. Gold colloid concentrations, C_0, pH, and conductivity of the diffusion inlet solutions.

Gold colloids (nm)	Gold colloid conc., C_0 (ppm)	3-Mercaptosuccinic acid conc. (μM)	pH	Conductivity (μS/cm)
2	4.6	4.0	8.5	1030
5	5.5	8.6	8.0	1190
15	5.5	2.0	7.4	940

https://doi.org/10.1346/CCMN.2010.0580408 Published online by Cambridge University Press

of gold colloids from the filter into the bentonite interface. After the two subsequent diffusion experiments, the diffusion cells were, therefore, frozen in liquid N_2 prior to dismantling, slicing, and addition of *aqua regia* in order to avoid contamination. Because the sensitivity and accuracy of the ICP-OES instrument is matrix dependent, duplicates of a bentonite reference sample that had not been in contact with gold colloids were also analyzed in order to determine possible background levels and estimate the measurement uncertainty of this method.

Microstructure investigation using low-angle XRD

Low-angle XRD, using a PANalytical X'Pert PRO instrument with CuKα radiation (1.542 Å) without a Ni filter, was used in reflection mode to measure the basal spacings of montmorillonite with a dry density of 0.5−1.0 g/cm^3. Two Soller slits (0.04 rad) and an automatic programmable divergence slit were used. The bentonite samples were water saturated for 4 weeks in three different ways. (1) One set of samples were water saturated under free conditions (FC) by mixing bentonite and water into a paste directly, which was then left in sealed syringes. Two other sets of samples were water saturated under volume-constricted conditions (VC) in the same diffusion cells as were used in the diffusion experiments (Figure 1b). (2) One set of volume-constricted samples (VC_1) was prepared exactly as in the diffusion experiments. (3) The other set of volume-constricted samples (VC_2) was water saturated mainly from one of the metallic frits, whereas the other metallic frit was covered with a perforated Kapton film in order to protect the bentonite surface from deformation when removing the frit. The VC samples were frozen prior to dismantling in order to avoid the suction effect. By comparing unfrozen and frozen/thawed samples as well as unfrozen/frozen/thawed samples, freezing and thawing failed to modify the XRD information. The treatments clearly did not alter the microstructure significantly and thawing is a surprisingly rapid process, confirming the findings by Norrish and Rausell-Colom (1991). During the measurements (<10 min) the samples were covered by a thin Kapton film in order to avoid drying effects. Directly after the measurements, the dry densities of the samples were measured gravimetrically, assuming a bentonite grain density of 2.8 g/cm^3 and a water density of 1 g/cm^3.

RESULTS AND DISCUSSIONS

The gold colloid stability of the 5- and 15-nm gold colloid inlet solutions was monitored qualitatively by UV-Vis spectroscopy during the diffusion experiment. The absorbance in the inlet solution decreased by 10−20% for the 5-nm gold colloids and by 35−60% for the 15-nm gold colloids. The TEM images of the inlet and outlet solutions were recorded half way through the experiment, 60 days into the first diffusion experiment using the 15-nm gold colloids. In the images of the inlet solutions, both individual and aggregated free gold colloids were observed, as well as gold colloids aggregated with bentonite residues. In images of the outlet solutions, no gold colloids could be found.

For the 2-nm gold colloids, no significant change in gold concentration was found in the inlet solutions during the experiment, confirming satisfactory colloid stability.

The sorption measurements preceding the diffusion experiments revealed a K_d of 43 cm^3/g for the thiol-treated colloids and 60 cm^3/g for the untreated (as received) gold colloids. These K_d values demonstrate that the negatively charged colloids were able to undergo sorption to some extent onto the negatively charged clay surfaces. Carboxylates are known to undergo sorption onto montmorillonite. The K_d values obtained are well in line with sorption data for succinic acid on montmorillonite as reported by Kang and Xing (2007). For succinic acid at the same volume to solid ratio as in the gold-colloid sorption experiments, the adsorbed ratio varied from 29 to 17% between pH 7 and 9, corresponding to K_d values of 58 and 34 cm^3/g, respectively. Using infrared spectroscopy, Kang and Xing (2007) found the binding type to be dominated by an outer-sphere interaction.

The gold concentrations in the filtered samples were, in general, similar to those in the unfiltered samples, ΔC_{Au} = ~0 (Figure 2a−c), meaning that no diffusion of gold colloids could be detected in the outlet solutions. The absence of detectable breakthrough after 4 months in the three diffusion experiments indicates that colloid transport through compacted bentonite was impossible or slow.

The gold concentrations measured in the bentonite pellets (Figure 3), *i.e.* the concentration profiles, revealed that, using the finite difference-based diffusion model *ANADIFF* (Eriksen and Jansson, 1996) and by varying the apparent diffusivity for $AuCl_4^-$ from 1×10^{-9} to 1×10^{-14} m^2/s and the sorption coefficient from 1 to 1000 cm^3/g (similar to D_a and K_d for Cl^- and I^-, Molera *et al.*, 2003), the residual $AuCl_4^-$ ($\leqslant$1 ppb) from the synthesis of the gold colloids clearly would not have been detected either in the outlet solutions or in the concentration profile analysis. Note that analysis of colloid diffusion must be based on the number of colloids per unit volume rather than the weight fraction when comparing colloids of different sizes. In general, the measured gold concentrations in the concentration profile analysis were very small. In the 15-nm gold colloid experiment, the first data point in the cell with greatest dry density (2.0 g/cm^3) was omitted due to leakage of gold colloids on the side of the metal frit, which was observed visually. The elevated gold concentrations of the 0.8 g/cm^3 and 1.2 g/cm^3 samples might be explained by the suction effect mentioned in

https://doi.org/10.1346/CCMN.2010.0580408 Published online by Cambridge University Press

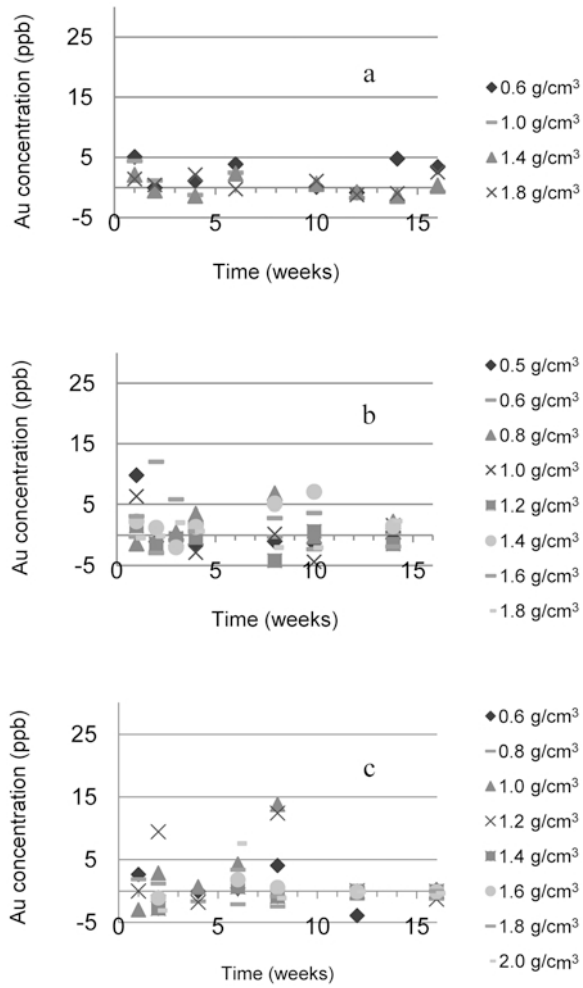


Figure 2. Gold colloid concentration, ΔC_{Au}, in the outlet solutions for the diffusion experiment using (a) 2-nm gold colloids, (b) 5-nm gold colloids, (c) 15-nm gold colloids.

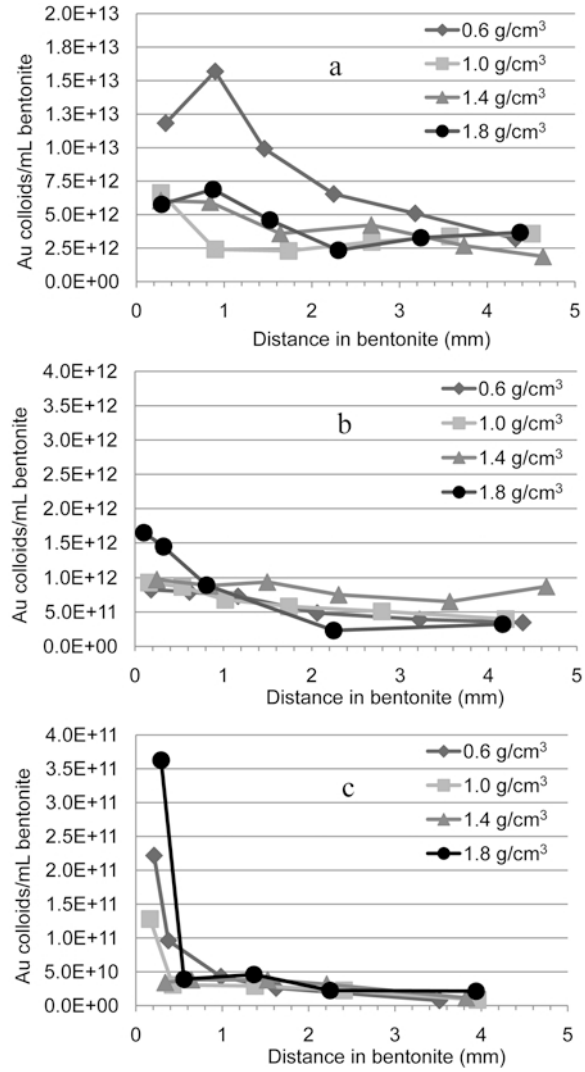


Figure 3. Gold concentration profiles in the compacted bentonite with different dry densities for the diffusion experiment using (a) 2-nm gold colloids, (b) 5-nm gold colloids, and (c) 15-nm gold colloids.

the experimental section. Only in the case of 2-nm gold colloids and bentonite compaction of 0.6 g/cm^3 could a clear exponential gold concentration gradient be observed (Figure 3a). The concentration profiles for the other compactions in the 2-nm gold colloid experiment (Figures 3b, 3c), as well as in the 5- and 15-nm gold colloid experiments, showed much less pronounced concentration gradients. The apparent concentration gradients can be explained by a background effect. In the bentonite reference sample, elevated background concentrations were found at 267.594 nm due to a nearby interfering emission line at 267.588 nm. The background concentration resulting from the bentonite reference sample as a function of bentonite mass (Figure 4), together with the gold concentrations measured in the 2 nm diffusion experiment, is explained as follows: the measured gold concentrations in the concentration profiles (Figure 3) are shown as the number of particles divided by the volume of bentonite, which is proportional to bentonite mass. Because the ratio of the background concentration to bentonite mass decreased with increasing bentonite mass (Figure 4) and as the mass of the bentonite slices in general increased with increasing distance from the inlet filters, the concentration profiles inevitably showed an apparent but small concentration gradient in all samples due to the background artifacts inherent to bentonite. The 2-nm gold colloids at the smallest compaction (0.6 g/cm^3) deviated from the measured background and from the results at greater compactions (Figure 4), as well as from the 5- and 15-nm gold colloid diffusion experiments (not shown), verifying that the 2-nm gold colloids were actually transported in the bentonite at that compaction. The results at greater compactions and from the 5- and

https://doi.org/10.1346/CCMN.2010.0580408 Published online by Cambridge University Press

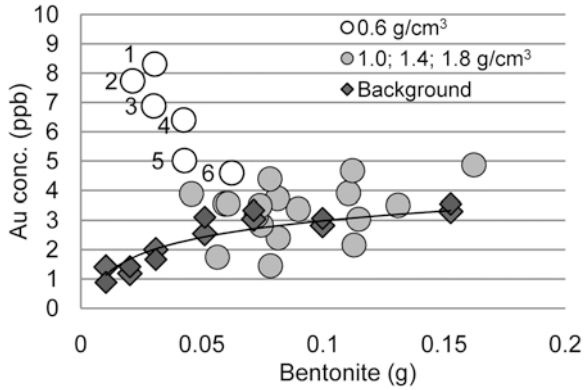


Figure 4. Measured gold concentrations as a function of bentonite mass. Circles show the gold concentrations for bentonite slices in the 2-nm diffusion experiment. Open circles at 0.6 g/cm^3 dry density (numbers indicating the order from the inlet filter). Filled circles at dry densities 1.0–1.8 g/cm^3. Gray diamonds show the measured bentonite background concentrations at 267.594 nm.

15-nm gold colloid diffusion experiments actually showed similar or increasing gold concentrations with bentonite mass contradicting any form of gold colloid diffusion because the mass of the bentonite slices generally increased with increasing distance from the inlet filters. Background artifacts inherent to the bentonite are the only possible explanation.

The apparent diffusivity of the 2-nm gold colloids at dry density 0.6 g/cm^3, corresponding to a montmorillonite density of 0.5 g/cm^3, was modeled using method I from Eriksen and Jacobsson (1984), and also using the *ANADIFF* code after subtracting the measured background concentrations from the concentration profile. Both methods gave similar apparent diffusivities but the *ANADIFF* code, which took filter effects into account, gave a slightly better fit (Figure 5).

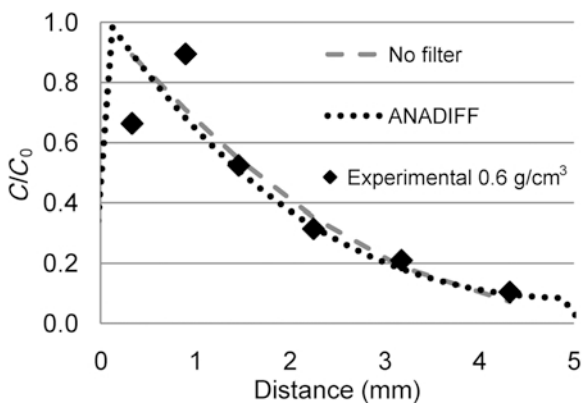


Figure 5. Experimental gold concentration profile in bentonite at dry density 0.6 g/cm^3 from the 2-nm diffusion experiment and corresponding modeled profiles. Black diamonds show the experimental points. The dashed gray curve shows the modeled curve without filter effects. The dashed black curve shows the concentration profile using *ANADIFF*.

The apparent diffusivity with filter effects taken into account (using the *ANADIFF* code) was $4.5\pm1\times10^{-13}$ m^2/s, while without filter effects it was $3\pm1\times10^{-13}$ m^2/s. Because parameters are unknown in this type of modeling, this value should only be interpreted as a rough estimate. For these 2-nm gold colloids at dry density of 0.6 g/cm^3, the ratio of the water diffusivity, D_W, (from the Stokes-Einstein relationship) and the apparent diffusivity, D_A, presented in this study was 450. This value can be compared with the corresponding factor for mobile anions and cations with small sorption capacity toward bentonite, which usually ranges from 3 to 30.

For each dry density, the low-angle XRD intensity (Figure 6) was set equal at 4.0°2θ to facilitate comparison. For all three different kinds of samples, with increasing water content (*i.e.* decreasing dry density), a gradual decrease in intensity due to crystalline swelling (3−4 water layers) was observed. Interestingly, only the VC_2 samples and the FC samples displayed diffraction peaks at lower angles due to osmotic swelling. The observed shoulder/peak resulting from osmotic swelling proved to be very sensitive to shearing of the sample surface. The reason why the VC_1 samples did not display a diffraction peak (*i.e.* having basal spacings which were too irregular to give rise to diffraction) as a result of osmotic swelling may depend, to some extent, on surface shearing when removing the metallic frits, as osmotic swelling was observed for the VC_2 samples at dry densities of 1.0−1.1 g/cm^3. The fact that osmotic swelling for the VC_2 samples was not observed at lesser dry densities, where the relative amount of osmotic swelling is expected to increase, implies that both the swelling pressure and water content affect the microstructural order because the FC samples, which were not subjected to any macroscopic swelling pressure, usually displayed well defined diffraction peaks due to osmotic swelling at dry densities of 0.6−1.0 g/cm^3. At 0.5 g/cm^3, diffraction peaks due to osmotic swelling could not be observed in the XRD profiles for any of the three sets of samples. In order to assess the impact of the accessory minerals on the low-angle XRD tracings at large water contents, two control samples consisting of 80% Na-montmorillonite and 20% Ca-montmorillonite (purified from MX-80 bentonite, Karnland *et al.* 2006) were water saturated and measured (not shown) in the same way as the VC_1 samples. For these synthetic bentonite samples with no accessory minerals, well defined diffraction peaks due to osmotic swelling were found. The apparent basal spacings of these samples were in line with the apparent basal spacings of the corresponding FC samples, taking the different montmorillonite content into account. (1) The accessory minerals may reduce the ordering, *i.e.* diffraction ability, of the montmorillonite layers subjected to osmotic swelling. (2) The interlayer distances due to osmotic swelling in samples water saturated under

https://doi.org/10.1346/CCMN.2010.0580408 Published online by Cambridge University Press

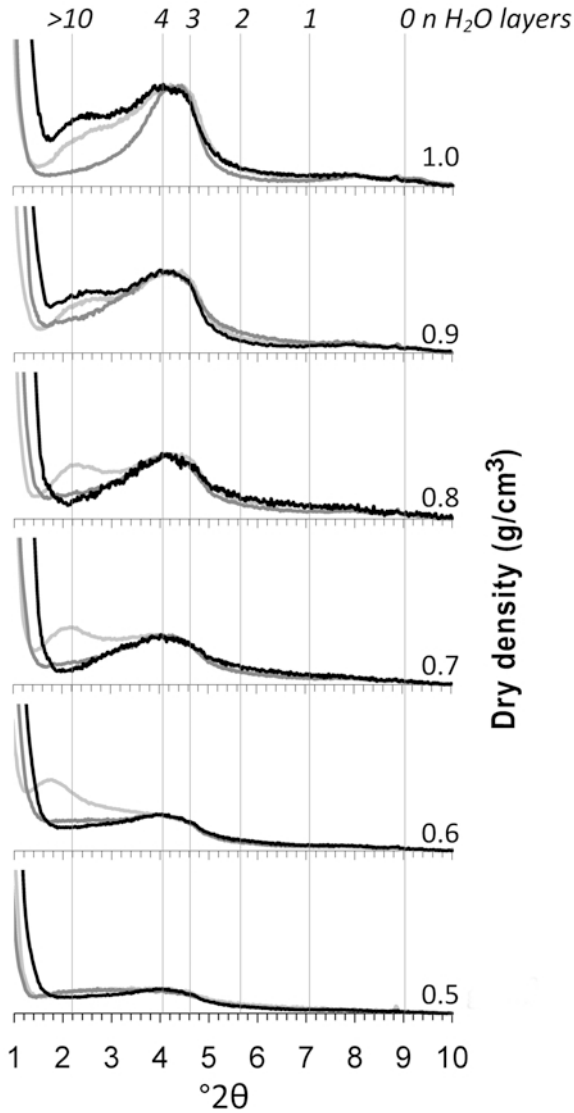


Figure 6. XRD profiles from bentonite samples at dry density 0.5−1.0 g/cm^3. FC samples are in light gray, VC_1 samples are in dark gray, and VC_2 samples are in black. Vertical lines represent the ideal positions of diffraction peaks corresponding to the *n* discrete H_2O layers.

constricted and free conditions at these water contents are similar on the nm scale.

The average interlayer distance in a bentonite sample depends primarily on the water content. As all the samples were equilibrated for a long time one can, therefore, assume that the osmotic swelling and the resulting interlayer distance in the FC sample at 0.6 g/cm^3 should be representative of the osmotic swelling and the corresponding interlayer distance for the VC samples at 0.6 g/cm^3.

The negatively charged gold colloids used in the present study were about the same size (for the 2-nm gold colloids) or larger than the interlayer distances between the individual montmorillonite layers in compacted bentonite. The 2-nm gold colloids displayed good colloid stability and so no change in size distribution during the experiment was expected. For the 5-nm gold colloids, a sufficiently large concentration of unaggregated colloids was assumed to have been maintained during the experiment in order to be detected in the bentonite if colloid transport of the 5-nm gold colloids had been possible. As no colloid transport of the 5-nm gold colloids was found, colloid transport of the 15-nm gold colloids would not be possible either, regardless of the colloid stability.

From the concentration profile analysis, the pore throat of the bentonite system at dry density 0.6 g/cm^3 is clearly >2 nm but <5 nm for negatively charged colloids. From the present data, at greater compaction, the pore throat of the bentonite system would probably be <2 nm for negatively charged colloids.

Considering the results from the low-angle XRD investigation, automatically ascribing the transport paths to only interparticle voids is probably unwise. As transport was only found at the greatest water content, where the average interlayer distance is the largest and considering that range distribution of interlayer spacings always exists, a larger fraction of the osmotic interlayer distances might be large enough for transport of negatively charged colloids despite electrostatic repulsion effects. Note that electrostatic repulsion effects must also exist to some extent in the interlayer voids due to the small bulk ionic strength used and the spill-over effect (Secor and Radke, 1985; Tombácz and Szekeres, 2004).

Regarding the interparticle voids, direct experimental evidence confirming the existence of interparticle voids in the mesopore range (2−50 nm; Gregg and Sing, 1982) in compacted water-saturated bentonite is scarce in the literature. Theoretical models used to predict radionuclide diffusion and hydraulic conductivity, which are based on a number of assumptions regarding the interparticle porosity, can be found in the literature.

Bourg *et al.* (2003) pointed out that for bentonite with dry density >1.4 g/cm^3, in the regime of crystalline swelling, the so-called 'free porosity' would in fact be substantial, and decrease linearly upon increasing dry density according to:

$$\varepsilon_{free} = 1 - 0.55\rho_{dry}$$

One precondition for this equation, however, is that the interlayer porosity increases with increasing dry density, which seems counter intuitive as the interlayer spacings, where most of the water is located (Norrish, 1954), decrease with increasing dry density. Suzuki *et al.* (2004) developed a parametric model to estimate the size of interparticle voids for particles arranged face to face, assuming planar and uniform geometry. Based on a basal spacing of 1.88 nm, the model gives void-size ranges of 6.0−11.1 nm and 1.2−1.4 nm for dry densities

https://doi.org/10.1346/CCMN.2010.0580408 Published online by Cambridge University Press

of 0.9 g/cm^3 and 1.35 g/cm^3, respectively, which is more or less in line with findings by Muurinen *et al.* (2004), who also assumed interparticle voids of similar sizes in their microstructural model. The volume fraction of the interparticle voids in the model by Suzuki *et al.* (2004) is estimated at 61% and 22%, respectively. Note, however, that this model requires the average number of montmorillonite layers in each stack to be known. Furthermore, neither the model of Suzuki *et al.* (2004) nor that of Muurinen *et al.* (2004) addressed the effects of osmotic swelling explicitly, possibly because they are based on low-angle XRD data from samples prepared in the same way as the VC_1 samples in the present study (which do not display diffraction due to osmotic swelling at small dry-density values).

Norrish (1954), on the other hand, showed that the average basal spacing for well oriented Na-montmorillonite samples is directly proportional to water content (see also Zhang and Low, 1989, and references therein). For well oriented Na-montmorillonite particles at a dry density of 0.6 g/cm^3, the interlayer distance was reported to be 3.4 nm, corresponding to ~11−12 water layers. Such an interlayer distance is identical to the maximum interlayer distance possible at that water content, meaning that the interparticle porosity for his (Norrish, 1954) well oriented montmorillonite was very small. For the bentonite used in the present study, due to random particle orientation, smaller smectite content, and the presence of accessory minerals, the interparticle porosity could be expected to be somewhat larger. The maximum interlayer distance at a specific water content for bentonite can be calculated as per Norrish (1954) for Na-montmorillonite, if the presence of accessory minerals is also taken into account. At dry density values of 1.0, 0.9, 0.8, 0.7, and 0.6 g/cm^3, the calculated maximum interlayer distance is ~2.0, 2.3, 2.8, 3.3, and 4.1 nm, respectively, assuming that the bentonite grain density and the average density of the accessory minerals is 2.8 g/cm^3 and a specific surface area for montmorillonite of 760 m^2/g (Karnland *et al.*, 2006). For a dry density of 0.6 g/cm^3, the maximum interlayer distance is close to the apparent osmotic interlayer distance of 4 nm. Note that the precise interlayer distances in these samples cannot be determined without proper XRD modeling, accounting for mixed layering, Lorentz polarization, and complex layer-structure functions, and which, to the authors' knowledge, is difficult at such large water contents. Similar interlayer spacings at slightly greater dry densities, however, have been reported in two recent small-angle X-ray scattering studies (Muurinen, 2009; Segad *et al.*, 2010). In these studies the interlayer distances of MX-80 bentonite due to osmotic swelling at dry densities 0.69 and 0.74 g/cm^3, respectively, was ~4 and 4.4 nm (basal spacings of 5 and 5.4 nm: A. Muurinen, M. Segad, pers. comm.). In the study by Muurinen (2009), the fraction of "free" montmorillonite layers at dry density of 0.69 g/cm^3 having basal spacings between 3 and 10 nm, as estimated by modeling the SAXS data, was 68%. Considering that the water content at dry density of 0.6 g/cm^3 is 20% greater than at 0.69 g/cm^3, this suggests, in accord with Norrish (1954), that the total porosity of bentonite at dry density of 0.6 g/cm^3 and low ionic strength will be dominated by the interlayer porosity due to osmotic swelling.

The fact that diffraction peaks due to osmotic swelling were not always observed at 0.6 g/cm^3 for the VC samples also implies that a large range of interlayer spacings exists. Due to the large interlayer distances found and the expected distribution of interlayer distances, the possibility of interlayer transport contributing to overall transport of the 2-nm gold colloids at 0.6 g/cm^3 cannot be ruled out.

For greater compactions and larger colloids, the results are in line with the results of Nowak (1984) and Kurosawa and Ueta (2001). The latter authors concluded that bentonite with dry density of at least 0.8 g/cm^3 would eliminate colloid diffusion.

The apparent diffusivity obtained in the present study for the 2-nm gold colloids is more than one order of magnitude less than the apparent diffusivities found by Wold and Eriksen (2007) and Iijima *et al.* (2009) for diffusion of small organic colloids at various compactions. Because the organic colloids are expected to be less charged than the gold colloids, they would be less subjected to electrostatic repulsion effects, leading to greater apparent diffusivities compared with the gold colloids. The greater apparent diffusivities of the humic and lignosulphonate colloids may also reflect the ability of the organic colloids to adapt their conformation to their surroundings, giving smaller colloids in terms of both size and charge.

To further investigate the microstructure and colloid diffusion in compacted bentonite, diffusion experiments using small and monodisperse 'water-like' nanoparticles or colloids should be carried out. In such experiments, the possible effect of 'anion exclusion' would be minimized. Suggested nanoparticles/colloids are organic macromolecules such as viruses or water-soluble gold colloids capped with thio-polymers.

SUMMARY AND CONCLUSIONS

Highly compacted bentonite will effectively prevent diffusion of inorganic colloids, as shown in this study for 2-, 5-, and 15-nm gold colloids. The absence of breakthrough curves agrees well with earlier experimental work using gold colloids of similar and larger sizes than those in this study. A significant number of gold colloids was only found for the smallest colloids (2 nm) at the smallest compaction value used (0.6 g/cm^3). The corresponding apparent diffusivity was on the order of ~5×10^{-13} m^2/s. Considering the large interlayer distances due to osmotic swelling in bentonite at such large water contents, as found in the low-angle XRD investigation (this study) and

https://doi.org/10.1346/CCMN.2010.0580408 Published online by Cambridge University Press

SAXS investigations found in the literature, one may speculate that the interlayer voids contribute to and may constitute pore throats in the overall colloid transport at 0.6 g/cm^3. For the larger gold colloids and/or greater compactions examined, colloid diffusion was effectively hindered by physical filtration due to the compact microstructure of bentonite.

ACKNOWLEDGMENTS

Financial support by the Swedish Nuclear Fuel and Waste Management Co. (SKB) is gratefully acknowledged. The authors are also grateful for valuable comments and suggestions by the reviewers.

REFERENCES

Bourg, I.C., Bourg, A.C.M., and Sposito, G. (2003) Modeling diffusion and adsorption in compacted bentonite: a critical review. *Journal of Contaminant Hydrology*, **61**, 293–302.

Devineau, K. Bihannic, I. Michot, L. Villiéras, F. Masrouri, F. Cuisinier, O. Fragneto, G., and Michau, N. (2006) In situ neutron diffraction analysis of the influence of geometric confinement on crystalline swelling of montmorillonite. *Applied Clay Science*, **31**, 76–84.

Enüstün, B.V. and Turkevich, J. (1963) Coagulation of colloidal gold. *Journal of the American Chemical Society*, **85**, 3317–3328.

Eriksen, T. and Jansson, M. (1996) Diffusion of I^-, Cs^+ and Sr^{2+} in compacted bentonite – Anion exclusion and surface diffusion. *SKB Technical Report*, TR-96-16, Swedish Nuclear Fuel and Waste Management Co., Stockholm, Sweden.

Ferrage, E., Lanson, B., Sakharov, B.A., and Drits, V.A. (2005) Investigation of smectite hydration properties by modeling experimental X-ray diffraction patterns: Part I. Montmorillonite hydration properties. *American Mineralogist*, **90**, 1358–1374.

Gregg, S.J. and Sing, K.S.W. (1982) *Adsorption, Surface Area and Porosity*, 2nd edition. Academic Press, London.

Iijima, K., Kurosawa, S., Tobita, M., Kibe, S., and Ouchi, Y. (2009) Diffusion behavior of humic acid in compacted bentonite: effect of ionic strength, dry density and molecular weight of humic acid. *Material Research Society Symposium Proceedings. Scientific Basis for Nuclear Waste Management* **XXXII**, 1124-Q05-04.

Janeba, D., Capkova, P., Weiss, Z., and Schenk, H. (1988) Characterization of intercalated smectites using XRD profile analysis in the low-angle region. *Clays and Clay Minerals*, **46**, 63–68.

Kang, S. and Xing, B. (2007) Adsorption of dicarboxylic acids by clay minerals as examined by in situ ATR-FTIR and ex situ DRIFT. *Langmuir*, **23**, 7024–7031.

Karnland, O., Olsson, S., Nilsson, U., and Sellin, P. (2006) Mineralogy and sealing properties of various bentonites and smectite rich materials. *SKB Technical Report*, TR-06-30, Swedish Nuclear Fuel and Waste Management Co., Stockholm, Sweden.

Kozaki, T., Fujishima, A., and Sato, S. (1998) Self-diffusion of sodium ions in compacted montmorillonite. *Nuclear Technology*, **121**, 63–69.

Kurosawa, S. and Ueta, S. (2001) Effect of colloids on radionuclide migration for performance assessment of HLW disposal in Japan. *Pure and Applied Chemistry*, **73**, 2027–2037.

Luckham, P.F. and Rossi, S. (1999) The colloidal and rheological properties of bentonite suspensions. *Advances in Colloid and Interface Science*, **82**, 43–92.

Molera, M., Eriksen, T., and Jansson, M. (2003) Anion diffusion pathways in bentonite clay compacted to different dry densities. *Applied Clay Science*, **23**, 69–76.

Moore, D.M. and Reynolds, R.C. Jr. (1997) *X-ray Diffraction and the Identification and Analysis of Clay Minerals*, 2nd edition. Oxford University Press, New York.

Muurinen, A. (2009) *Studies on the chemical conditions and microstructure in the reference bentonites of alternative buffer materials project (ABM) in Äspö*. POSIVA Working Report 2009-42.

Muurinen, A., Karnland, O., and Lehikoinen, J. (2004) Ion concentration caused by an external solution into the porewater of compacted bentonite. *Physics and Chemistry of the Earth*, **29**, 119–127.

Norrish, K. (1954) The swelling of montmorillonite. *Discussions of the Faraday Society*, **18**, 120–134.

Norrish, K. and Rausell-Colom, J.A. (1962) Effect of Freezing on the swelling of clay minerals. *Clay Minerals Bulletin*, **5**, 9–16.

Nowak, E.J. (1984) Diffusion of colloids and other waste species in brine-saturated backfill materials. *Materials Research Society Symposium Proceedings, Scientific Basis for Nuclear Waste Management* VII, **26**, 59–68.

Saiyouri, N., Tessier, D., and Hicher, P.Y. (2004) Experimental study of swelling in unsaturated compacted clays. *Clay Minerals*, **39**, 469–479.

Secor, R.B. and Radke, C.J. (1985) Spillover of the diffuse double layer on montmorillonite particles. *Journal of colloid and Interface Science*, **103**, 237–244.

Segad, M., Jönsson, B., Åkesson, T., and Cabane, B. (2010) Ca/Na-montmorillonite: structure, forces and swelling properties. *Langmuir*, **26**, 5782–5790.

Suzuki, S., Sato, H., Ishidera, T., and Fujii, N. (2004) Study on anisotropy of effective diffusion coefficient and activation energy for deuterated water in compacted sodium bentonite. *Journal of Contaminant Hydrology*, **68**, 23–37.

Tombácz, E. and Szekeres, M. (2004) Colloidal behavior of aqueous montmorillonite suspensions: the specific role of pH in the presence of indifferent electrolytes. *Applied Clay Science*, **27**, 75–94.

Vaia, R.A. and Liu, W. (2002) X-ray powder diffraction of polymer/layered silicate nanocomposites: model and practice. *Journal of Polymer Science: Part B: Polymer Physics*, **40**, 1590–1600.

Vilks, P., Stroes-Gascoyne, S., Goulard, M., Haveman, S.A., and Bachinski, D.B. (1998) The release of organic material from clay-based buffer materials and its potential implications for radionuclide transport. *Radiochimica Acta*, **82**, 385–391.

Wold, S. and Eriksen, T. (2007) Diffusion of humic colloids in compacted bentonite. *Physics and Chemistry of the Earth*, **32**, 477–484.

Zhang, Z.Z. and Low, P.F. (1989) Relation between the heat of immersion and the initial water content of Li-, Na-, and K-montmorillonite. *Journal of Colloid and Interface Science*, **133**, 461–472.

Zhu, T., Vasilev, K., Kreiter, M., Mittler, S., and Knoll, W. (2003) Surface modification of citrate-reduced colloidal gold nanoparticles with 2-mercaptosuccinic acid. *Langmuir*, **19**, 9518–9525.

(*Received 22 October 2008; revised 2 June 2010; Ms. 221; A.E. R. Dohrmann*)

https://doi.org/10.1346/CCMN.2010.0580408 Published online by Cambridge University Press